IEEE Access
Multidisciplinary | Rapid Review | Open Access Journal

Received July 27, 2019, accepted August 4, 2019, date of publication August 7, 2019, date of current version August 21, 2019.

Digital Object Identifier 10.1109/ACCESS.2019.2933657

Consequent Pole Permanent Magnet Vernier Machine With Asymmetric Air-Gap Field Distribution

HUAWEI ZHOU[1], (Member, IEEE), WEIGUO TAO[1], CHENG ZHOU[1], YANXIN MAO[1], GUANG-JIN LI[2], (Senior Member, IEEE), AND GUOHAI LIU[1], (Senior Member, IEEE)

[1]School of Electrical and Information Engineering, Jiangsu University, Zhenjiang 212013, China
[2]Department of Electronic and Electrical Engineering, University of Sheffield, Sheffield S1 4DE, U.K.

Corresponding author: Huawei Zhou (zhouhuawei@ujs.edu.cn)

This work was supported in part by the National Natural Science Foundation of China under Project 51877100, and in part by the Priority Academic Program Development of Jiangsu Higher Education Institutions.

ABSTRACT In recent years, permanent magnet vernier (PMV) machines have been attracting more and more attention due to the inherently exhibited advantages such as high torque density and simple mechanical structure. In this paper, a consequent pole (CP) PMV machine with single-layer concentrated winding is proposed. The novelty is that the asymmetric air-gap field distribution is introduced to improve its working harmonics and to reduce the PM consumption. By employing a CP structure, the flux density amplitude can be enhanced. Moreover, due to uneven distribution of modulator poles on the armature teeth and fault tolerant teeth, the number of periods of modulator poles is only half of that of the stator teeth. Then, significant improvement in flux density working harmonics can be achieved. Furthermore, the superior electromagnetic decoupling capability can be achieved by introducing the fault-tolerant teeth. The relevant electromagnetic performance such as flux density, back electromotive forces, cogging torque and on-load torque have been calculated by using finite-element analyses, which have also been validated by experiments.

INDEX TERMS Asymmetric air-gap field distribution, consequent pole, fault-tolerant, flux density working harmonic, permanent magnet vernier machine.

I. INTRODUCTION

Due to the advantages such as superior torque density, high efficiency, and simple mechanical structure, permanent magnet (PM) machines have been widely used in industry and electric vehicle [1]–[5]. One special type of PM machine, the permanent magnet vernier (PMV) machine can achieve even higher torque density compared with other conventional PM machines mainly due to their operation principle based on magnetic gearing effect [6], [7]. Therefore, these PMV machines are mainly employed in the low speed large torque direct-drive applications such as electric vehicle, wind power generator and ship propulsion [8]–[10].

For conventional PMV machines, the orders of modulated flux density harmonics, which equal to the number of stator pole pairs, are always considered while the other harmonic components are neglected [11]. Thus, the flux density harmonics are not effectively utilized, which offsets the advantage of high torque density. Torque capability and quality of PMV machines were analyzed in [12], [13]. It shows that the working harmonics in air-gap flux density can increase torque capability, and the other undesirable flux density harmonic components have serious negative impact on machine's electromagnetic performance such as increasing the torque ripple and also core losses [14], [15]. Therefore, it is important to increase the working harmonic components and eliminate the undesirable harmonic components in flux density. In order to enhance the torque capability of PMV machines, multiple flux density working harmonics were introduced in [16], [17]. For a PMV machine with double-layer concentrated windings, by adjusting the pitch angle of modulator poles, the number of periods of modulator poles can be equal to the number of stator teeth. Then, based on the magnetic gearing principle, more flux density working harmonics can be generated, thus improving the torque density [17], [18]. However, when the same method is employed

The associate editor coordinating the review of this manuscript and approving it for publication was Xiaodong Sun.

for a PMV machine with single-layer windings, although the number of periods of modulator poles is still equal to the number of stator teeth, the produced desirable working flux density harmonics are insufficient. Thus, this method cannot be used in the PMV machine with single-layer windings.

Recently, the consequent pole (CP) concept is introduced. Compared with the conventional PM machines with N-S poles rotor, the machines with CP rotors have homopolar PMs (either N-pole or S-pole) [19]. Such arrangement can provide higher back electromotive forces (EMFs) and also larger torque capability for the machines even with smaller PM volume [20], [21]. This increase in torque capability is mainly due to the asymmetric air-gap field distribution [22], [23].

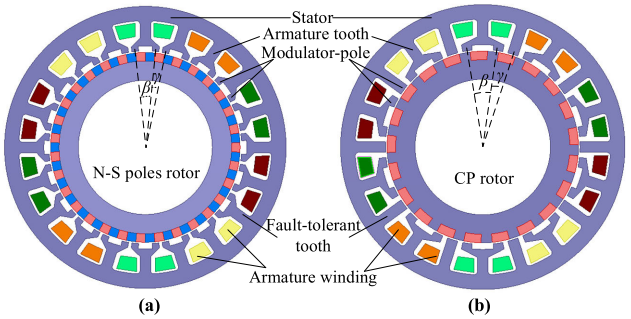

FIGURE 1. Cross sections of (a) existing PMV machine with N-S poles rotor and (b) proposed PMV machine with CP rotor.

In this paper, to enhance the torque capability and fault-tolerance of the PMV machines and also to reduce the magnet consumption, a novel five-phase PMV machine with CP rotor and also single-layer concentrated windings is proposed, as shown in Fig.1. Compared with three-phase machine, multiphase machine can achieve higher efficiency, lower torque ripple and better power splitting [24]. The main contribution of this paper therefore lies in the introduction of asymmetric air-gap field distribution in the proposed PMV machine with CP rotor. It can bring two main advantages: 1) combined with the CP structure, the air-gap flux density can be enhanced leading to lower PM consumption; 2) more working harmonics in the air-gap flux density can be obtained with special uneven distribution of modulator poles.

II. MACHINE TOPOLOGY WITH BIASED AIR-GAP FIELD DISTRIBUTION

As shown in Fig. 1, all the radially magnetized PMs in CP structure are homopolar. As a result, the open-circuit fluxes due to PMs pass through the stator and the salient rotor core, and finally return to the PMs, as shown in Fig. 2. Hence, all the salient rotor iron poles between PMs are magnetized to another polarity and can be regarded as the virtual poles. Furthermore, in order to reduce the end winding length and the associated extra copper loss and also to enhance the fault-tolerant capability, the fractional slot concentrated single-layer windings and fault-tolerant teeth are adopted. Based on

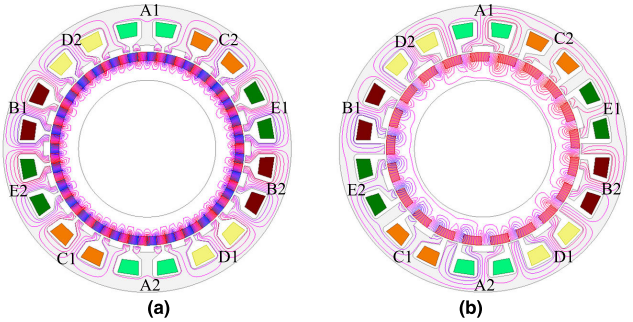

FIGURE 2. Open-circuit flux line distribution of (a) existing PMV machine with N-S poles rotor and (b) proposed PMV machine with CP rotor.

such arrangement, to modulate more desirable flux density harmonics, the pitch angle β is designed to be unequal to the slot opening angle γ. Moreover, the armature and fault-tolerant teeth are all called stator teeth. If they have saturation problem, their width needs to be increased. This can be decided after appropriately optimizing the stator teeth. However, the slot area needs to be maintained constant to keep the copper loss unchanged during the optimizing process. The detailed parameters of the proposed machine are summarized in Table 1.

TABLE 1. Optimized parameters of existing machine and proposed machine.

Parameter	Existing machine with N-S poles rotor	Proposed machine with CP rotor
Stator outer diameter, mm	168	
Stator inner diameter, mm	115	
Rotor outer diameter, mm	113	
Rotor inner diameter, mm	80	
Stack length, mm	100	
Slot number	20	
Stator teeth number	20	
Air-gap length, mm	1	
Tooth width, mm	6.3	
Rotating speed, rpm	300	
Rated peak current, A	10	
PM thickness, mm	5	
PM volume, cm^3	169.6	112.8
Rotor pole pairs	31	21
Armature pole pairs	9	9
Modulator poles	40	30
Pole arc ratio	1	0.66
Modulator tooth width, mm	4	5.6
Pitch angle β, deg	12	18
Slot opening angle γ, deg	6	9
Power factor	0.52	0.68

To simplify the analyses, the open-circuit PM air-gap flux density distribution without considering the slotting effect and the leakage flux is shown in Fig. 3. For the existing machine with N-S poles rotor, the flux density distribution is symmetrical, and its magnitude can be expressed as

$$B_{n-s} = \frac{B_r}{1 + \frac{g\mu_r}{h_m}} \tag{1}$$

where B_r is the remanent flux density of PMs, μ_r is the PM recoil permeability ($\approx$1), g is the air-gap length, and h_m is the

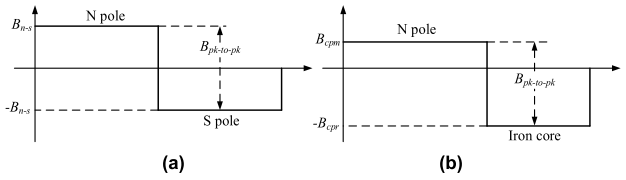

FIGURE 3. Air-gap flux density distribution. (a) N-S pole. (b) CP.

PM thickness. The air-gap flux density can be represented as

$$B_{n-s}(\theta_s, t) = \sum_i \frac{4B_{n-s}}{i\pi} \sin\left(\frac{i}{2}\pi\right) \cdot \cos\left[i\left(P_r\theta_s - \omega t\right)\right] \quad (2)$$

where θ_s is the mechanical angle, ω is the electrical angular speed, and P_r is the PM pole pairs. The relationship of the ω and P_r can be expressed as

$$\omega = \frac{\pi n P_r}{30} \quad (3)$$

where n is the rotor mechanical speed. However, for the proposed machine with CP rotor, the flux density distribution is asymmetric, the amplitudes B_{cpm} and B_{cpr} are respectively expressed as

$$B_{cpm} = \frac{B_r}{1 + \frac{g\mu_r}{h_m(1-\alpha)}} \quad (4)$$

$$B_{cpr} = \frac{\alpha}{1-\alpha} B_{cpm} \quad (5)$$

where α is the PM pole arc to pole pitch ratio. The air-gap flux density can be given as

$$B_{cp}(\theta_s, t) = \sum_i \frac{2B_{cpm}}{i\pi(1-\alpha)} \sin(i\pi\alpha) \cos\left[i\left(P_r\theta_s - \omega t\right)\right] \quad (6)$$

The relationship between B_{n-s} and B_{cp} can be expressed as

$$B_{cpm} + B_{cpr} - 2B_{n-s} = \frac{\left(2\alpha - 1 - \frac{g\mu_r}{h_m}\right) B_r}{\left(1 - \alpha + \frac{g\mu_r}{h_m}\right)\left(1 + \frac{g\mu_r}{h_m}\right)} \quad (7)$$

It can be found that the equivalent fundamental amplitude and peak-to-peak value of air-gap flux density of the existing machine with N-S poles rotor and the proposed machine with CP rotor can be obtained if satisfying

$$\begin{cases} 2\alpha - 1 - \dfrac{g\mu_r}{h_m} \geq 0 \\ \dfrac{g\mu_r}{h_m}[\sin(\alpha\pi) - 2] + 2\alpha - 2 + \sin(\alpha\pi) \geq 0 \end{cases} \quad (8)$$

Based on the aforementioned analyses, it can be found that the air-gap flux density of the proposed machine is biased and it can be adjusted to achieve higher value according to (8). For example, Fig. 4 (a) shows the comparison of open-circuit air-gap flux density distribution of the machine with N-S poles rotor and the machine with CP rotor. It can be seen that air-gap flux density of the machine with CP rotor is larger, though the PM consumption is significantly reduced. Hence, the higher fundamental amplitude of the machine with CP rotor can be obtained, as shown in Fig. 4 (b).

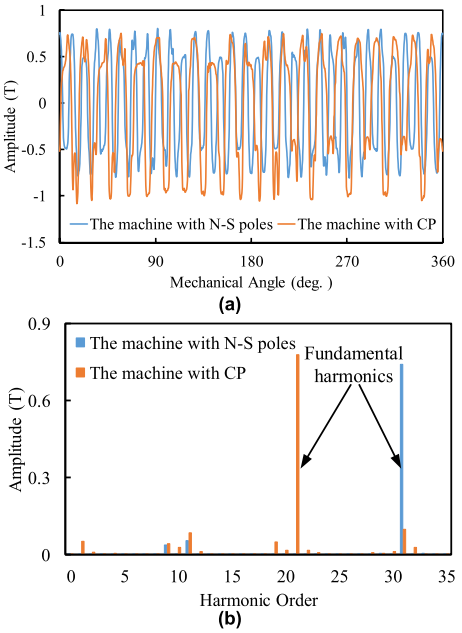

FIGURE 4. Comparison of open-circuit air-gap flux densities of machine with N-S poles rotor and machine with CP rotor. (a) Waveform. (b) Spectra.

III. OPERATION PRINCIPLE

A. FLUX DENSITY HARMONICS DUE TO PMS

Compared with the conventional PM machines, the rotor pole pairs of PMV machines are not equal to armature winding pole pairs. The relationship of the pole pairs of PMV machines always satisfies

$$P_f = P_r \pm P_s \quad (9)$$

where P_f, P_r, and P_s are the modulator pole number, the pole pair numbers of rotor and armature windings, respectively. Since the principle between the PMV machine and magnetically geared machine are almost the same, for a magnetically geared machine, there is an outer air-gap between the modulator poles and stator core, the PMV machine is essentially equivalent to the corresponding magnetically geared machine when the outer air-gap is infinitely small [17]. In the outer air-gap, the torque will be generated when the modulated PM harmonics interact with the corresponding winding harmonics. Hence, the modulated flux density harmonics in the outer air-gap are investigated.

Due to the CP PM rotor, all the PMs have the same polarity. According to the magnetic circuit theory, the magnetomotive forces (MMFs) generated by rotor PMs can be assumed to be square wave. The period of square wave is $2\pi/P_r$. Thus the PM MMFs can be expressed in Fourier series, as

$$\begin{aligned} F_c(\theta_s, t) &= \frac{\alpha B_r h_m}{\mu_0\mu_r} \\ &\quad + \sum_{j=1,2,3,\cdots} \frac{2}{j\pi} \frac{B_r h_m}{\mu_0\mu_r} \sin(j\alpha\pi) \cos\left(jP_r\theta_s - j\omega t\right) \\ &= F_0 + \sum_{j=1,2,3,\cdots} F_j \cos\left(jP_r\theta_s - j\omega t\right) \end{aligned} \quad (10)$$

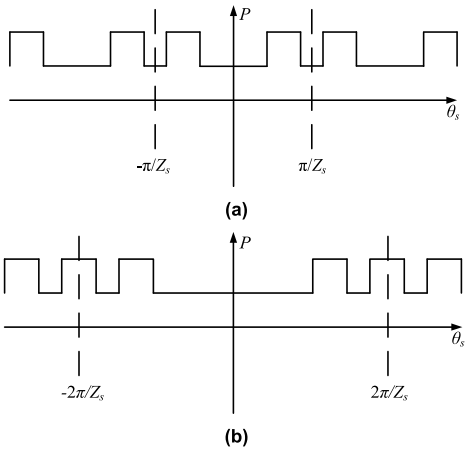

FIGURE 5. Air-gap permeance function of (a) existing machine with N-S poles rotor and (b) proposed machine with CP rotor.

where F_0 is the DC component, and F_i is the amplitude of i^{th} MMF harmonic.

Fig. 5 (a) shows the air-gap permeance model of the existing machine, where Z_s is the stator teeth number and is equal to the stator slot number, i.e. 20. It can be found that the number of permeance periods is equal to that of the stator teeth, and the pitch angle is unequal to the slot opening angle. However, for the proposed machine, due to the unequal number of modulator poles distributed on the armature teeth and the fault tolerant teeth as well as the unequal pitch and slot opening angles, its number of permeance periods is only half of that of the stator teeth, as shown in Fig. 5 (b). The air-gap permeance function can be expressed in Fourier series, as

$$\Lambda(\theta_s) = \Lambda_0 + \sum_{i=1,2,3,\cdots} \Lambda_i \cos(iZ\theta_s) \tag{11}$$

where Λ_0 and Λ_i are the DC component and the amplitude of the i^{th} permeance harmonic, respectively; Z is the stator teeth number in the existing machine, but it is only half of that of the stator teeth in the proposed machine. Therefore, with this special structure, the air-gap permeance harmonics of the proposed machine are more enriched.

When only considering the constant and fundamental components (i.e. $j = 1$) of the MMFs, the modulated air-gap flux density of proposed machine can be expressed as (12). It should be noted that the $(P_r)^{\text{th}}$, $(P_r \pm iP_f)^{\text{th}}$ flux density harmonics are the inherent harmonics in the proposed machine, which also exist in all PMV machines. However, the $(iZ)^{\text{th}}$ and the $(P_r \pm iZ)^{\text{th}}$ harmonics are the newly generated harmonics and the speed of which are $\omega/(iZ)$ and $\omega/|P_r \pm iZ|$, respectively. And, it can be seen from Table 2 that the $(iZ)^{\text{th}}$ and the $(P_r \pm iZ)^{\text{th}}$ flux density harmonics are generated in the proposed machine. The main reason is that the period number of the permeance in the proposed machine is only half of that of the existing machine. Fig. 6 shows

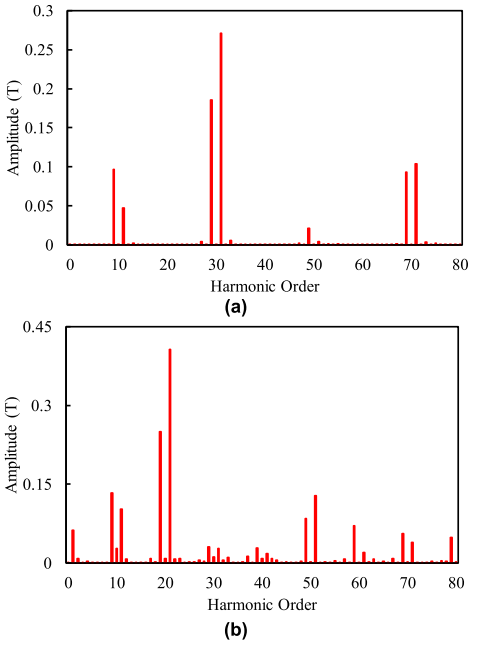

FIGURE 6. Spectra of simulated air-gap flux density due to PMs. (a) Existing PMV machine with N-S poles rotor. (b) Proposed PMV machine with CP rotor.

TABLE 2. Modulated flux density harmonics due to PMs.

Pole pairs	Existing machine with N-S poles rotor	Proposed machine with CP rotor	Speed
P_r	31	21	ω/P_r
P_r+iP_f	71	51	$\omega/(P_r+iP_f)$
P_r-iP_f	-9,-49	-9,-39,-69	$-\omega/\lvert P_r-iP_f\rvert$
iZ	-	10,20,30	$\omega/(iZ)$
P_r-iZ	11, -9,-29,-49,-69	1,11, -9,-19,-29,-39,-49,-59,-69,-79	$\omega/\lvert P_r-iZ\rvert$ $-\omega/\lvert P_r-iZ\rvert$
P_r+iZ	51,71	31,41,51,61,71	$\omega/(P_r+iZ)$

the simulated results of the harmonic spectra of flux density due to PMs. It should be noted that the amplitudes of the $(iZ)^{\text{th}}$ flux density harmonics in the proposed machine are much smaller than that of the other flux density harmonics. Thus, it proves that the harmonic orders are consistent with those predicted in Table 2, where the symbol "-" represents the negative rotating direction. Therefore, with this special structure, more flux density harmonics are introduced in the proposed machine.

$$\begin{aligned} B_g(\theta_s, t) = {} & \Lambda_0 [F_0 + F_1 \cos(P_r\theta_s - \omega t)] \\ & + \sum_{i=1,2,3,\cdots} F_0\Lambda_i \cos(iZ\theta_s) \\ & + \sum_{i=1,2,3,\cdots} \frac{F_1\Lambda_i}{2} \cos[(P_r + iZ)\theta_s - \omega t] \\ & + \sum_{i=1,2,3,\cdots} \frac{F_1\Lambda_i}{2} \cos[(P_r - iZ)\theta_s - \omega t] \end{aligned} \tag{12}$$

B. FLUX DENSITY HARMONICS DUE TO ARMATURE WINDINGS

The MMF of five-phase symmetrical windings can be expressed as

$$F_w = \sum_{v=1}^{\infty} \left\{ \sum_{n=0,2,4,6,8} \frac{1}{2} F_v \cos\left[v\theta_s - \omega t + (1-v)\frac{n\pi}{5} \right] + \sum_{n=0,2,4,6,8} \frac{1}{2} F_v \cos\left[v\theta_s + \omega t - (1+v)\frac{n\pi}{5} \right] \right\} \quad (13)$$

where F_v is the amplitude of the v^{th} MMF harmonic. It can be noted that the five-phase symmetrical windings only generate $|10k+1|^{th}(k = 0, \pm1, \pm2, \pm3\ldots)$ MMF harmonics, where "-" represents the negative rotating direction. Therefore, according to the magnetic gear principle, the $|10k+1|^{th}$ flux density harmonics in the outer air-gap are generated by stator windings, and the speed is $\omega/|10k+1|$. The armature flux density harmonics are listed in Table 3, and the simulated results of the armature flux density spectra are shown in Fig. 7. It can be seen that the harmonic orders of the armature flux density are consistent with theoretical predictions.

TABLE 3. Flux density harmonics due to armature windings.

Pole pairs	Harmonic order	Speed
$10k$+1(k=-1,-2…)	-9, -19, -29, -39…	$-\omega/\|10k+1\|$
$10k$+1(k=0, 1, 2…)	1, 11, 21, 31…	$\omega/(10k+1)$

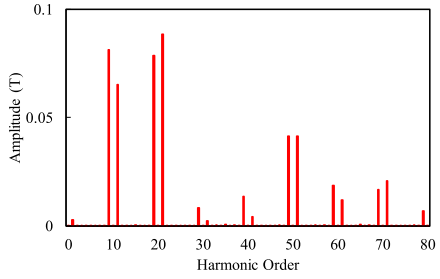

FIGURE 7. Spectra of simulated air-gap flux density due to armature windings.

Therefore, except for the $(iZ)^{th}$ harmonics, the order, the speed and rotating direction of flux density harmonics due to PMs are the same as those due to armature windings in the proposed machine. Thus, these harmonics of flux density due to PMs will interact with the corresponding flux density harmonics due to armature winding, and steady electromagnetic torque can then be generated. In addition, due to special distribution of the asymmetric air-gap field, more flux density working harmonics are generated, leading to potentially much higher torque capability.

IV. ELECTROMAGNETIC PERFORMANCE

A. BACK-EMF

The general expression of back-EMF can be given as

$$e = -\frac{d}{dt}\left[r_g L_{stk} \int_0^{2\pi} B_g(\theta_s, t) \left(\sum_{v=1,3,5\cdots} -N_v \sin v\theta_s \right) d\theta_s \right] \quad (14)$$

where r_g is the radius of the air-gap, L_{stk} is the active axial length, N_v is the v^{th} harmonic amplitude of the winding function. Substituting (12) into (14), the fundamental back EMF of phase-A can be expressed as

$$e_a = r_g L_{stk} \pi \omega \Lambda_0 F_1 N_{v=P_r} \cos \omega t + \sum_{i=1,2,3\cdots} \frac{1}{2} r_g L_{stk} \pi \omega \Lambda_i F_1 N_{v=P_r \pm iZ} \cos \omega t \quad (15)$$

It is worth noticing that except the $(iZ)^{th}$ flux density harmonics due to PMs, all the other flux density harmonics, e.g. the P_r^{th}, $(P_r \pm iZ)^{th}$, $(P_r \pm iP_f)^{th}$, will contribute to the fundamental back-EMF.

When j in (10) is equal to even number, jP_r and $jP_r \pm iZ$ are even-order. Thus, the $(jP_r)^{th}$ and $(jP_r + iZ)^{th}$ flux density harmonics are generated due to the even-order PM MMF harmonics, but their amplitudes are quite small. According to (14), the integral value of them is zero, i.e. the even-order harmonics in back-EMFs are zero. Therefore, there are only odd-order harmonics in back-EMFs.

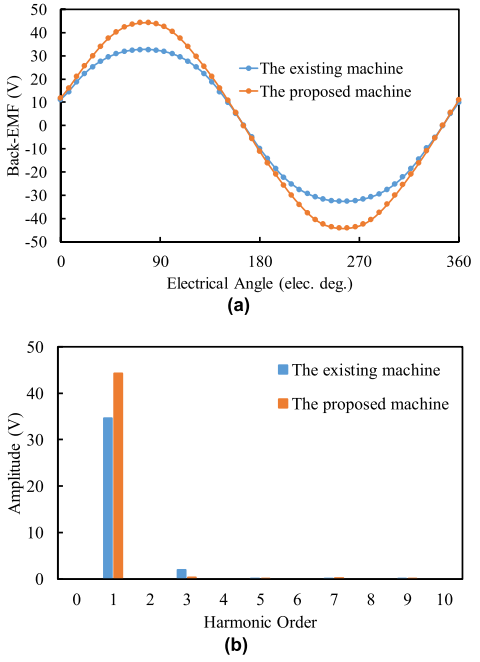

FIGURE 8. Comparison of no-load back-EMF of phase-A. (a) Waveforms. (b) Spectra.

Fig. 8 shows the comparison of no-load back-EMFs of the two machines. It can be seen that the back-EMF amplitude of the proposed machine is 35.8% higher than that of the existing machine, but its higher order harmonics are much lower, leading to potentially higher average torque and lower torque ripple.

B. COGGING TORQUE

Cogging torque is generated by the interaction between the PMs and stator teeth-slot. The pole arc to pole pitch ratio has an important effect on the cogging torque. The PMs in N-S

array are surface-mounted on the rotor, the pole arc of PMs is relatively fixed. However, the pole arc of PMs in CP array can be adjusted easily. The optimized pole arc to pole pitch ratio of the proposed machine is 0.66, the waveforms and spectra of cogging torque of the existing and proposed machines are shown in Fig. 9. The peak value of the existing and proposed machines is 259mNm and 65mNm, respectively. Thus, the cogging torque of the proposed machine is significantly reduced.

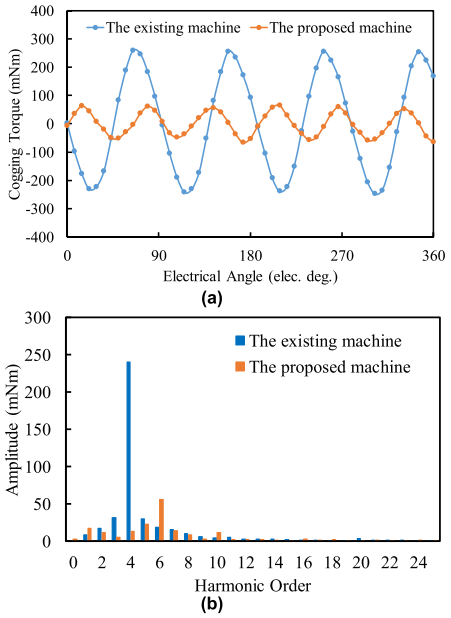

FIGURE 9. Comparison of cogging torque between existing and proposed machines. (a) Waveform. (b) Spectra.

C. TORQUE CAPABILITY

The average torque can be expressed as

$$T_e = \frac{5}{2} r_g L_{stk} \pi P_r I_{\max} \Lambda_0 F_1 N_{v=P_r} + \frac{5}{2} r_g L_{stk} \pi P_r I_{\max} \sum_{i=1,2,3\cdots} \frac{1}{2} \Lambda_i F_1 N_{v=P_r \pm iz} \quad (16)$$

where $I_{\max}$ is the amplitude of armature current. It can be seen that all the flux density working harmonics involved in the fundamental back-EMF engage in the effective torque production. The parameter k is the modulator pitch ratio, which is defined as

$$k = \frac{\beta P_f}{2\pi} \quad (17)$$

The torque optimization of the proposed machine with modulator pitch ratio k is presented in Fig. 10. It can be seen that the torque increases with the increase in k. When k reaches 1.5, the maximum torque is obtained, and then β is calculated to be 18 degrees. Fig. 11 shows the optimal torque comparison of the two machines. It can be seen that the average torque of the proposed machine is 23.6% higher than that of the existing machine, and also the torque waveform is smoother due to the lower back-EMF harmonics

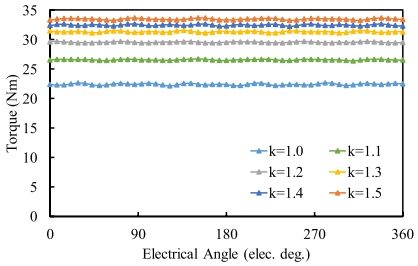

FIGURE 10. Torque vs modulator pitch ratio k in proposed machine with CP rotor at rated peak current.

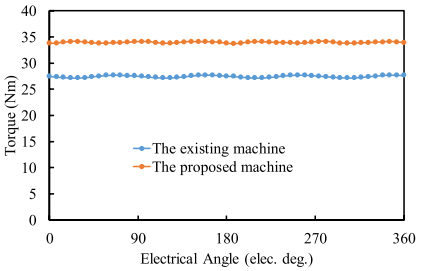

FIGURE 11. Torque comparison between existing and proposed machines at rated peak current.

(see Fig. 8) and also much smaller cogging torque (see Fig. 9). Additionally, it should be noted that the increase ratio of the average torque of the proposed machine is lower than that of the no-load back-EMF. This is mainly due to the fact that the virtual poles during on-load operation are saturated. This is one of the main drawbacks of the CP rotor due to the reduced effective air-gap length.

D. FAULT-TOLERANT CAPABILITY

The electromagnetic coupling characteristic between phases can be indicated by the mutual-inductance, and the fault-tolerant capability can be investigated by the ratio of the mutual- to self-inductances. Since phase-A is adjacent to phase-C and phase-D in spatial structure, as shown in Fig. 2, the mutual-inductances L_{ac} and L_{ad} are larger than the mutual-inductances L_{ab} and L_{ae}, as shown in Fig. 12. On the other hand, due to the CP rotor, the permeability of core is much larger than that of PM and then the salient pole structure is generated. Hence, the inductance ripple of the proposed machine is larger than that of the existing machine. The maximum mutual-inductances of the existing and proposed machines are 0.0083mH and 0.159mH, respectively. And the maximum ratios of mutual- to self-inductance are 0.15% and 1.63%, respectively. Thus, the ratio of mutual- to self-inductance of the proposed machine is slightly larger than that of the existing machine, but the value is still small. Therefore, the excellent fault-tolerant capability still can be achieved in the proposed machine.

E. POWER FACTOR

Asymmetric flux distribution is incorporated with CP structure, which allows the higher main flux and lower leakage flux to be achieved with less PM consumption.

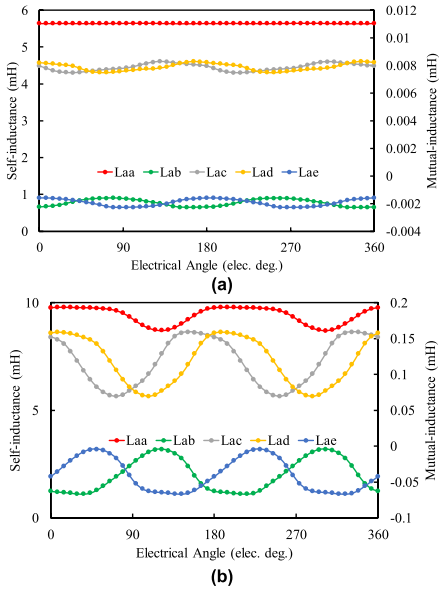

FIGURE 12. Mutual- and self-inductances of (a) existing machine with N-S poles rotor and (b) proposed machine with CP rotor.

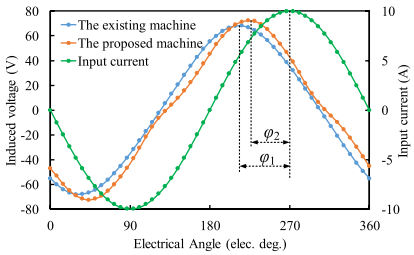

FIGURE 13. Waveforms of Induced voltages and rated current.

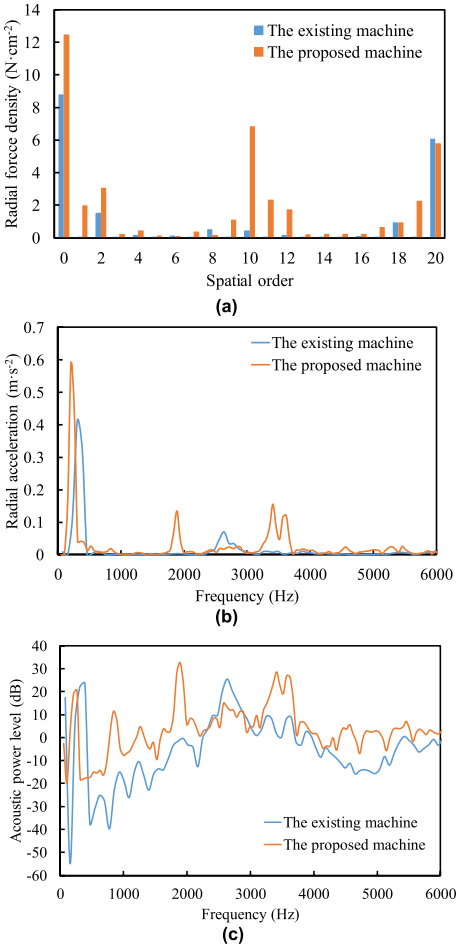

FIGURE 14. Comparison of (a) radial force density, (b) radial acceleration, and (c) acoustic power level.

Combined with the biased flux modulation theory, the uneven distribution of modulator poles on the armature teeth and fault tolerant teeth, more flux density working harmonics are generated. Hence, higher back-EMF and torque capability of the proposed machine are achieved compared with those of the existing machine. The waveforms of induced voltage and rated current are shown in Fig. 13. It can be found that the power factor angle (φ_2) of the proposed machine is smaller than that (φ_1) of the existing machine. It can be calculated that the power factors of the proposed and existing machines are 0.68 and 0.52, respectively. Therefore, the power factor can be improved by adopting the proposed topology.

F. VIBRATION AND NOISE

Fig. 14 shows the radial force density, radial acceleration, and acoustic power level of the existing and proposed machines. It can be seen that the maximum radial accelerations of the existing and proposed machines are 0.41 $m{\cdot}s^{-2}$ and 0.59 $m{\cdot}s^{-2}$, respectively, which are mainly due to the 2nd order radial electromagnetic force harmonic. The total acoustic power levels of the existing and proposed machines are 30.64 dB and 36.39 dB, respectively. Therefore, though the vibration and noise of the proposed machine are slightly larger than that of the existing machine, the value is still small. This means that the vibration and noise resulted from the asymmetric field are slight.

V. EXPERIMENTAL VALIDATION

The proposed machine is prototyped for the verification of aforementioned analyses. The machine assembly and test rig are shown in Fig. 15. The magnetic power brake is utilized to generate a load torque for the test prototype.

Under the rated speed of 300 r/min, the phase back-EMF and average torque versus q-axis current for the proposed machine are measured and compared with FE in Figs. 16 and 17. It can be seen that the amplitudes of the FE-predicted and measured back-EMFs are 44.32 V and 44.11 V, respectively. The amplitude of the 3rd harmonic of the measured result (1.38 V) is slightly higher than that of the FE-predicted one (0.3 V) due to the limited manufacturing process. Otherwise, the measured result agrees well with the FE-prediction. Since the manufacturing tolerances and end-effects are not included in the FE analyses, the measured torque is slightly lower than the FE-prediction. However, the difference between them is within the acceptable error range.

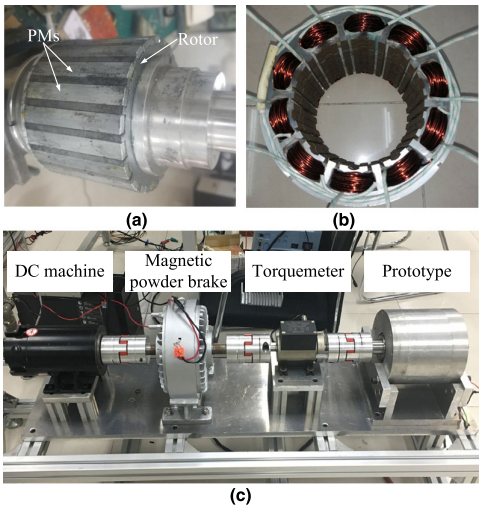

FIGURE 15. Test rig setup. (a) Stator. (b) Rotor. (c) Test bench.

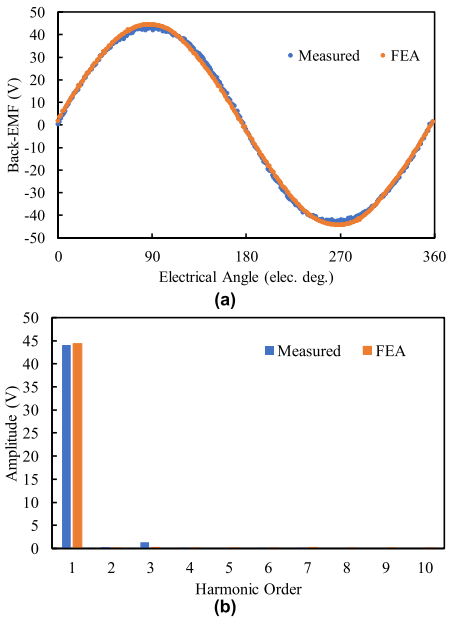

FIGURE 16. Comparison of measured and predicted back-EMFs at 300 r/min.

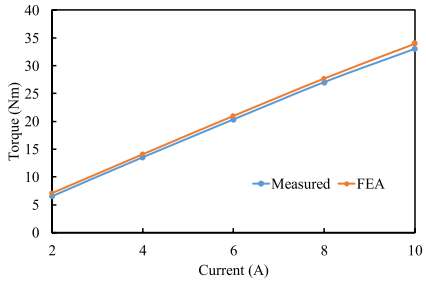

FIGURE 17. Measured and predicted average torques vs peak current.

Due to the fault-tolerant design, the stator windings have little electromagnetic coupling. Fig. 18 shows the measured waveforms of short-circuit current and no-load back-EMFs. The short-circuit current is limited by the large stator

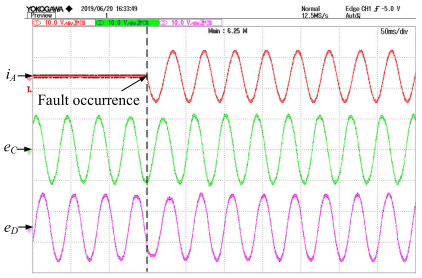

FIGURE 18. Impact of short-circuit (phase-A) on back EMFs at no-load condition (10A/div, 10V/div, 50ms/div).

winding inductance. It can be seen that when a short-circuit fault occurs in the phase-A, the back-EMFs of the two adjacent phases are nearly not affected, as expected.

VI. CONCLUSION

In this paper, to enhance torque and fault-tolerant capabilities whilst with reduced PM consumption, a CP PMV machine with single-layer concentrated windings is proposed. Combined with the biased flux modulation theory, the flux density of the proposed machine is improved by adopting the CP structure. In addition, much more flux density working harmonics are generated by adopting the special uneven distribution of modulator poles. Therefore, compared with the existing machine, the proposed machine can obtain larger flux density, 35.8% higher no-load Back-EMFs, 30.7% higher power factor, 23.6% higher torque with lower torque ripple, but with only 66.5% PM consumption. Furthermore, the ratio of the mutual- to self-inductance is only 1.63%, thus excellent fault-tolerant capability can be achieved. However, due to smaller effective air-gap length, the CP rotor is easy to be saturated. It will be investigated in the future.

REFERENCES

[1] H. Yang, S. Lyu, Z. Q. Zhu, H. Lin, S. Wang, S. Fang, and Y. Huang, "Novel dual-stator machines with biased permanent magnet excitation," *IEEE Trans. Energy Convers.*, vol. 33, no. 4, pp. 2070–2080, Dec. 2018.

[2] N. Baloch, J.-W. Kwon, M. Ayub, and B.-I. Kwon, "Low-cost dual-mechanical-port dual-excitation machine for washing machine application," *IEEE Access*, vol. 7, pp. 87141–87149, 2019.

[3] Z. Shi, X. Sun, Y. Cai, Z. Yang, G. Lei, Y. Guo, and J. Zhu, "Torque analysis and dynamic performance improvement of a PMSM for EVs by skew angle optimization," *IEEE Trans. Appl. Supercond.*, vol. 29, no. 2, Mar. 2019, Art. no. 0600305.

[4] X. Sun, C. Hu, J. Zhu, S. Wang, W. Zhou, Z. Yang, G. Lei, K. Li, B. Zhu, and Y. Guo, "MPTC for PMSMs of EVs with multi-motor driven system considering optimal energy allocation," *IEEE Trans. Magn.*, vol. 55, no. 7, Jul. 2019, Art. no. 8104306.

[5] X. Sun, C. Hu, G. Lei, Y. Guo, and J. Zhu, "State feedback control for a PM hub motor based on grey wolf optimization algorithm," *IEEE Trans. Power Electron.*, to be published. doi: 10.1109/TPEL.2019.2923726.

[6] Y. Liu, H. Y. Li, and Z. Q. Zhu, "A high-power factor Vernier machine with coil pitch of two slot pitches," *IEEE Trans. Magn.*, vol. 54, no. 11, Nov. 2018, Art. no. 8105405.

[7] Z. Q. Zhu and Y. Liu, "Analysis of air-gap field modulation and magnetic gearing effect in fractional-slot concentrated-winding permanent-magnet synchronous machines," *IEEE Trans. Ind. Electron.*, vol. 65, no. 5, pp. 3688–3698, May 2018.

[8] X. Zhao, S. Niu, and W. Fu, "A novel Vernier reluctance machine excited by slot PMs and zero-sequence current for electric vehicle," *IEEE Trans. Magn.*, vol. 55, no. 6, Jun. 2019, Art. no. 8102405.

[9] Z. Song, C. Liu, and H. Zhao, "Quantitative comparison of distinct dual-stator permanent magnet Vernier machines for direct-drive applications," *IEEE Trans. Magn.*, vol. 55, no. 7, Jul. 2019, Art. no. 8104806.
[10] B.-T. Kim, "Design method of a direct drive permanent magnet Vernier generator for a wind turbine system," *IEEE Trans. Ind. Appl.*, to be published. doi: 10.1109/TIA.2019.2923717.
[11] B. Kim and T. A. Lipo, "Operation and design principles of a PM Vernier motor," *IEEE Trans. Ind. Appl.*, vol. 50, no. 6, pp. 3656–3663, Nov. 2014.
[12] D. Li, R. Qu, J. Li, L. Xiao, L. Wu, and W. Xu, "Analysis of torque capability and quality in Vernier permanent-magnet machines," *IEEE Trans. Ind. Appl.*, vol. 52, no. 1, pp. 125–135, Jan./Feb. 2016.
[13] X. Ren, D. Li, R. Qu, Z. Yu, and Y. Gao, "Investigation of spoke array permanent magnet Vernier machine with alternate flux bridges," *IEEE Trans. Energy Convers.*, vol. 33, no. 4, pp. 2112–2121, Dec. 2018.
[14] B. Lee, Z. Q. Zhu, and L. Huang, "Investigation of torque production and torque ripple reduction for six-stator/seven-rotor-pole variable flux reluctance machines," *IEEE Trans. Ind. Appl.*, vol. 55, no. 3, pp. 2510–2518, May/Jun. 2019.
[15] M. Baghayipour, A. Darabi, and A. Dastfan, "Detailed analytical method for predicting the steady-state time variations and entire harmonic contents of principal performance characteristics in a non-slotted axial flux permanent magnet motor, considering a precise iron loss model," *IET Electr. Power Appl.*, vol. 12, no. 3, pp. 308–322, Mar. 2018.
[16] Z. Z. Wu and Z. Q. Zhu, "Analysis of air-gap field modulation and magnetic gearing effect in switched flux permanent magnet machines," *IEEE Trans. Magn.*, vol. 51, no. 5, May 2015, Art. no. 8105012.
[17] T. Zou, D. Li, R. Qu, D. Jiang, and J. Li, "Advanced high torque density PM Vernier machine with multiple working harmonics," *IEEE Trans. Ind. Appl.*, vol. 53, no. 6, pp. 5295–5304, Nov./Dec. 2017.
[18] W. Zhang, S. Huang, J. Gao, R. Li, and L. Dai, "Electromagnetic torque analysis for all-harmonic-torque permanent magnet synchronous motor," *IEEE Trans. Magn.*, vol. 54, no. 11, Nov. 2018, Art. no. 8206405.
[19] Y. Li, H. Yang, H. Lin, S. Lyu, and Z. Pan, "Comparative study of stator-consequent-pole permanent magnet machines with different stator-slot configurations," *IEEE Trans. Magn.*, vol. 55, no. 7, Jul. 2019, Art. no. 8106308.
[20] H. Yang, L. Qin, S. Fang, H. Lin, and S. Wang, "A parallel consequent pole reluctance machine with bipolar coil flux-linkage," *IEEE Access*, to be published. doi: 10.1109/ACCESS.2019.2917943.
[21] D. Li, R. Qu, J. Li, and W. Xu, "Consequent-pole toroidal-winding outer-rotor Vernier permanent-magnet machines," *IEEE Trans. Ind. Appl.*, vol. 51, no. 6, pp. 4470–4481, Nov./Dec. 2015.
[22] H. Yang, Z. Q. Zhu, H. Lin, H. Li, and S. Lyu, "Analysis of consequent-pole flux reversal permanent magnet machine with biased flux modulation theory," *IEEE Trans. Ind. Electron.*, to be published. doi: 10.1109/TIE.2019.2902816.
[23] F. Li, K. Wang, J. Li, and H. Y. Sun, "Electromagnetic performance analysis of consequent-pole PM machine with asymmetric magnetic Pole," *IEEE Trans. Magn.*, vol. 55, no. 6, Jun. 2019, Art. no. 8103205.
[24] H. Zhou, G. Liu, W. Zhao, X. Yu, and M. Gao, "Dynamic performance improvement of five-phase permanent-magnet motor with short-circuit fault," *IEEE Trans. Ind. Electron.*, vol. 65, no. 1, pp. 145–155, Jan. 2018.

HUAWEI ZHOU (M'16) received the B.Sc. and M.Sc. degrees in control engineering from Jiangsu University, Zhenjiang, China, in 2003 and 2006, respectively, and the Ph.D. degree in electrical engineering from the Graduate University of Chinese Academy of Sciences, Beijing, China, in 2012.

He has been with Jiangsu University, since 2003, where he is currently an Associate Professor with the School of Electrical Information Engineering. From 2017 to 2018, he was a Visiting Academic Scholar with the Department of Electronic and Electrical Engineering, University of Sheffield, Sheffield, U.K. His teaching and research interests include electric machines design, PM motor drives for electric vehicles and electromagnetic suspension, fault-tolerance analysis, and intelligent control.

WEIGUO TAO received the B.Sc. degree in electrical engineering from Yancheng Teachers University, Yancheng, China, in 2017. He is currently pursuing the M.Sc. degree in electrical engineering with Jiangsu University, Zhenjiang, China.

His current research interests include PM machine design and control.

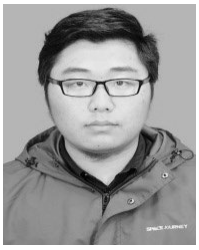

CHENG ZHOU received the B.Sc. degree in electrical engineering from the Yancheng Institute of Technology, Yancheng, China, in 2017. He is currently pursuing the M.Sc. degree in electrical engineering with Jiangsu University, Zhenjiang, China.

His current research interests include drive and control of PM motors.

YANXIN MAO received the M.Sc. degree from the Wuhan Institute Physics and Mathematics, Chinese Academy of Sciences, China, in 2004, and the Ph.D. degree in electrical engineering from Jiangsu University, Zhenjiang, China, in 2018.

She has been with Jiangsu University, since 2004. Her research interests include vibration and acoustic noise of permanent magnet machines.

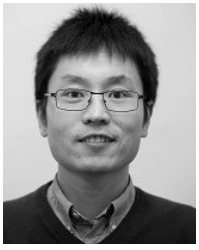

GUANG-JIN LI (M'10–SM'16) received the B.Eng. degree from Wuhan University, China, in 2007, the M.Sc. degree from the University of Paris XI, France, in 2008, and the Ph.D. degree from the Ecole Normale Supérieure (ENS) de Cachan, Paris, France, in 2011, all in electrical and electronic engineering.

He joined the Electrical Machines and Drives (EMD) Group, University of Sheffield, Sheffield, U.K., in 2012, as a Postdoctoral Research Associate, where he was appointed as an Assistant Professor, in 2013. He is currently an Associate Professor in electrical machines with the EMD Group, University of Sheffield. His main research interests include the design, fault analysis, and thermal management of electrical machines for renewable energy, automotive, and more electrical aircrafts.

GUOHAI LIU (M'07–SM'15) received the B.Sc. degree in electrical engineering from Jiangsu University, Zhenjiang, China, in 1985, and the M.Sc. and Ph.D. degrees in control engineering from Southeast University, Nanjing, China, in 1988 and 2002, respectively.

He has been with Jiangsu University, since 1988, where he is currently a Professor and the Dean of the School of Electrical Information Engineering. From 2003 to 2004, he was a Visiting Professor with the Department of Electronic and Electrical Engineering, University of Sheffield, Sheffield, U.K. He holds 30 patents in his research areas. He has authored or coauthored over 200 technical papers and 4 textbooks. His teaching and research interests include electrical machines, and motor drives for electric vehicles and intelligent control.